

ON THE MODELLING OF STEADY GENERALIZED NEWTONIAN FLOWS IN A 3D CORONARY BYPASS

Jan Vimmr, Alena Jonášová*

Blood's non-Newtonian behaviour is investigated in an idealized coronary 3D bypass model, which includes both the proximal and distal parts of the occluded native artery and the connected end-to-side bypass graft. Considering the blood to be a generalized Newtonian fluid, the shear-dependent viscosity is given by two well-known macroscopic non-Newtonian models (the Carreau-Yasuda model and the modified Cross model). Both non-Newtonian steady flow fields are analyzed with regard to the bypass geometry and are compared with the case of the Newtonian fluid. In order to perform all numerical simulations, we developed an incompressible Navier-Stokes solver based on the pseudo-compressibility approach and on the cell-centred finite volume formulation of the central explicit fourth-stage Runge-Kutta time stepping scheme defined on unstructured hexahedral computational grid.

Key words: coronary occluded artery, bypass model, non-Newtonian flow, Carreau-Yasuda model, Cross model, FVM, unstructured hexahedral grid

1. Introduction

The investigation of bypass hemodynamics is one of the topical themes in biomechanics because of the need to better understand the influence of local hemodynamics on the vascular wall in order to explain and also to predict a possible failure of implanted bypass grafts. The damage of blood cells, thrombus formation and development of intimal hyperplasia at the distal anastomosis are the main consequences, which result from the unnatural bypass geometry applied in the high-pressure bloodstream.

Until now quite many studies dealt with the problem of bypass hemodynamics, whereas it is possible to separate their objectives into two categories. The first one investigates the influence of various geometric and flow parameters on the resulting blood flow. One of the studies, [7], considered the steady blood flow through an occluded bypass model for various inlet Reynolds numbers and junction angles. Similar problem with the exception of stenosed native artery was introduced in [1], where one of the main objectives was to state the importance of so-called distance of grafting on the blood flow downstream from the artery narrowing. The second category of published studies is devoted to the improvement of the anastomosis geometry, which is known to be connected with the development of intimal hyperplasia in implanted bypass grafts. For example, the connection between the distal native artery and the bypass graft in the form of autologous vein cuff (Miller cuff), was already clinically tested on several patients with interesting conclusions. In order to support the experiments, the benefits of this surgical technique were discussed in several studies, e.g. [5] and [9].

* Ing. J. Vimmr, Ph.D., Ing. A. Jonášová, Department of Mechanics, Faculty of Applied Sciences, University of West Bohemia, Univerzitní 22, 306 14 Plzeň, Czech Republic

Concerning the problem of blood flow through a complete idealized 3D bypass model with either occlusion or stenosis, we performed several numerical simulations in the past, [10], whereas we assumed the blood to be a Newtonian fluid. Since the consideration of shear-dependent viscosity in connection with bypass hemodynamics is one of the less investigated problems, the main objective of the study presented here is to improve our existing computational model with the consideration of blood's non-Newtonian behaviour.

Regarding the wide variety of shear-thinning viscosity models used for human blood, one of the most often applied non-Newtonian model is probably the power-law model as is shown in [4]. The authors modelled an unsteady blood flow through the distal part of bypass with results implying a significant role of bypass/anastomosis geometry. Another study, [2], investigated the blood's non-Newtonian effects in a bypass model with 75 % stenosis applying the Carreau-Yasuda model with regard to different grafting distances and various inlet flow rates.

In the last ten years, the growing popularity of non-power-law viscosity models in connection with numerical simulation of blood flow through medium-sized arteries, was noted. Therefore, this article introduces the application of two well-known macroscopic non-Newtonian models, the Carreau-Yasuda model and the modified Cross model, in comparison to the Newtonian flow. The new original numerical results obtained by own developed computational software, represent the investigation of steady non-Newtonian blood flow through an idealized occluded 3D bypass model, which compared to the common practice, consists of both proximal and distal parts of the native artery and of the connected end-to-side bypass graft. In order to approach this problem adequately, physiological parameters (artery diameter and inlet Reynolds number) corresponding to the coronary artery were applied.

2. Problem formulation

Compared to the usual practice to model only the distal part of the bypass, in this study, we present a complete idealized 3D bypass model, which includes both the proximal and distal parts of the damaged native artery and the connected end-to-side bypass graft with the junction angle 45° . The modelled bypass corresponds to the in medicine applied coronaro-coronary bypass with following average physiological parameters: $D_{\text{artery}} = 0.0033$ m, $Re_{\text{inlet}} = 230$. The graft diameter is set equal to the diameter of the artery, i.e. $D_{\text{artery}} = D_{\text{graft}}$, whereas the length of native artery is $L = 0.05$ m. In practice, the most of applied bypass grafts are either venous or synthetic with negligible elastic properties. Therefore, we assume the model walls to be impermeable and rigid.

The flow restriction inside the native artery, which in our case is represented by an occlusion, is modelled as a wall blocking the direct flow through the artery. In Fig. 1 (left),

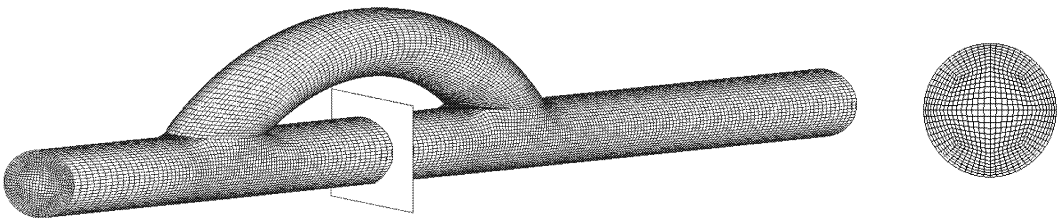


Fig.1: Computational grid with marked artery occlusion modelled as a wall (left); computational grid in the cross-section (right)

the applied unstructured hexahedral computational grid is shown including the marked occlusion position. For the purpose of obtaining hexahedral cells in the entire bypass model, the software Altair Hypermesh was used, whereas much attention was paid to the needed refinement in the wall vicinity, Fig. 1 (right), in order to resolve the boundary layer with sufficient accuracy. Although such computational grid may be very useful for the later analysis of recirculation zones by the bypass walls, it involves relatively complex generation in the anastomosis region considering the condition in the form of hexahedral cells. Therefore, a partly manual technique in combination with the algorithms of the software Altair Hypermesh had to be applied in order to achieve the grid connection between the native artery and the bypass graft.

Blood's rheological properties are influenced by many factors such as hematocrit and plasma protein concentration. Since it is impossible to consider the effect of all of them in a numerical simulation and since our investigation is restricted to blood flow in medium-sized arteries, we describe the fluid viscosity only as the function of shear rate. For this purpose, we apply two well-known macroscopic viscosity models, which enable us to model the blood's non-Newtonian behaviour by low shear rate values:

- the Carreau-Yasuda model

$$\eta(\dot{\gamma})^{(1)} = \eta_{\infty}^{(1)} + (\eta_0^{(1)} - \eta_{\infty}^{(1)}) \left[1 + (\lambda^{(1)} \dot{\gamma})^m \right]^{\frac{n-1}{m}}, \quad (1)$$

- the modified Cross model

$$\eta(\dot{\gamma})^{(2)} = \eta_{\infty}^{(2)} + (\eta_0^{(2)} - \eta_{\infty}^{(2)}) \left[1 + (\lambda^{(2)} \dot{\gamma})^b \right]^{-a}, \quad (2)$$

where $\lambda^{(k)}$, $k = 1, 2$ is the characteristic relaxation time, $\eta_0^{(k)}$ and $\eta_{\infty}^{(k)}$, $k = 1, 2$ are the zero shear viscosity and the infinite shear viscosity, respectively. The remaining parameters m , n , a , b are used in order to control the transition to the lower Newtonian range. In our numerical simulations, we applied following positive parameters:

- $\eta_{\infty}^{(1)} = 3.45 \times 10^{-3}$ Pa.s, $\eta_0^{(1)} = 56 \times 10^{-3}$ Pa.s, $\lambda^{(1)} = 1.1902$ s, $m = 1.25$, $n = 0.22$, see [6];
- $\eta_{\infty}^{(2)} = 3.5 \times 10^{-3}$ Pa.s, $\eta_0^{(2)} = 160 \times 10^{-3}$ Pa.s, $\lambda^{(2)} = 8.2$ s, $a = 1.23$, $b = 0.64$, see [8].

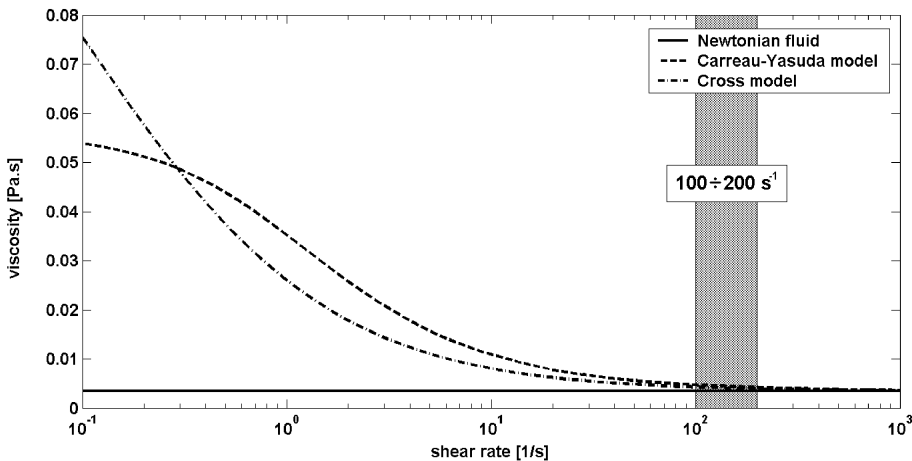


Fig. 2: Dependence of blood viscosity on shear rate described by the Carreau-Yasuda model and the modified Cross model

According to the source articles, all parameters mentioned here were derived from two independent viscometric experiments using dissimilar blood samples. In order to distinguish between both non-Newtonian models, the dependence of viscosity on shear rate is displayed in Fig. 2 by applying the given parameters. For comparison, the solid line in the graph represents the viscosity of the Newtonian fluid, which in this study was set equal to $\eta = \eta_{\infty}^{(1)} \doteq \eta_{\infty}^{(2)}$. From the obtained curves, we can deduce that for higher values of shear rate $\dot{\gamma}$ ($100\text{--}200\text{s}^{-1}$) the values of molecular viscosity $\eta(\dot{\gamma})$ evaluated by either the Carreau-Yasuda model or the Cross model are almost equal to the viscosity of the Newtonian fluid. Considering the relatively high inlet Reynolds number corresponding to the coronary artery ($Re_{\text{inlet}} = 230$), it is possible to assume that the differences between the non-Newtonian and Newtonian flow fields in our case will be probably very small. On the contrary by low shear rates, the graph implies significant viscosity differences between the Newtonian and non-Newtonian fluids, which should be notable in the flow fields consisting of recirculation and low-velocity zones.

3. Mathematical model of steady incompressible generalized Newtonian fluid flow

In this study, the 3D blood flow in large and medium-sized arteries is considered to be an isothermal laminar flow of an incompressible fluid with the density $\varrho = 1050\text{ kg m}^{-3}$ and with the constant molecular viscosity $\eta = 3.45 \times 10^{-3}\text{ Pas}$ in the case of Newtonian flow or with the shear-dependent molecular viscosity $\eta(\dot{\gamma})^{(k)}$, $k = 1, 2$ given either by the Carreau-Yasuda model (1) or by the modified Cross model (2), respectively, in the case of non-Newtonian flow. Applying the Einstein's summation convention, the governing equations for incompressible generalized Newtonian flow in a bounded computational domain $\Omega \subset \mathbb{R}^3$ and in a time interval $(0, \mathcal{T})$, $\mathcal{T} > 0$ constitute the non-linear system of the incompressible Navier-Stokes (NS) equations written in non-conservative form

$$\frac{\partial v_i}{\partial y_i} = 0, \quad (3)$$

$$\frac{\partial v_i}{\partial t} + v_j \frac{\partial v_i}{\partial y_j} + \frac{\partial P}{\partial y_i} = \frac{\partial}{\partial y_j} \left[\frac{\eta(\dot{\gamma})^{(k)}}{\varrho} \left(\frac{\partial v_i}{\partial y_j} + \frac{\partial v_j}{\partial y_i} \right) \right], \quad (4)$$

where $i, j = 1, 2, 3$. For solving the steady flow problem, the pseudo-compressibility method [3] is applied. Hence, the system of the incompressible NS equations (3)–(4) can be rewritten in the conservative pseudo-transient compact flux vector form as

$$\frac{\partial \mathbf{w}}{\partial t} + \sum_{s=1}^3 \frac{\partial \mathbf{F}_s^{\text{I}}(\mathbf{w})}{\partial y_s} = \sum_{s=1}^3 \frac{\partial \mathbf{F}_s^{\text{V}}(\mathbf{w})}{\partial y_s} \quad \text{in } \Omega \times (0, \mathcal{T}). \quad (5)$$

The vector \mathbf{w} of conservative variables and the inviscid and viscous flux vectors $\mathbf{F}_s^{\text{I}}(\mathbf{w})$ and $\mathbf{F}_s^{\text{V}}(\mathbf{w})$, respectively, are defined as

$$\mathbf{w} = (w_1, w_2, w_3, w_4)^{\text{T}} \equiv (P, v_1, v_2, v_3)^{\text{T}} \in \mathbb{R}^4, \quad (6)$$

$$\mathbf{w} = \mathbf{w}(\mathbf{y}, t), \quad \mathbf{y} = (y_1, y_2, y_3)^{\text{T}} \in \Omega, \quad t \in (0, \mathcal{T}),$$

$$\mathbf{F}_s^{\text{I}}(\mathbf{w}) = (\beta^2 v_s, v_1 v_s + P \delta_{1s}, v_2 v_s + P \delta_{2s}, v_3 v_s + P \delta_{3s})^{\text{T}}, \quad s = 1, 2, 3, \quad (7)$$

$$\mathbf{F}_s^{\text{V}}(\mathbf{w}) = \frac{\eta(\dot{\gamma})^{(k)}}{\varrho} \left(0, \frac{\partial v_1}{\partial y_s}, \frac{\partial v_2}{\partial y_s}, \frac{\partial v_3}{\partial y_s} \right)^{\text{T}}, \quad s = 1, 2, 3, \quad k = 1, 2. \quad (8)$$

Here v_s are the Cartesian components of the velocity vector $\mathbf{v} = (v_1, v_2, v_3)^T$ in the directions y_s , δ_{ij} is the Kronecker delta, p is the pressure, $P = p/\varrho$ and the parameter β represents the pseudo-speed of sound of the system (5) transformed by the pseudo-compressibility method.

According to $Re_{\text{inlet}} = U_{\text{ref}} D_{\text{ref}} \varrho_{\text{ref}} / \eta_{\text{ref}} = 230$, where $\eta_{\text{ref}} \equiv \eta = \eta_{\infty}^{(1)} \doteq \eta_{\infty}^{(2)} = 3.45 \times 10^{-3}$ Pas, $D_{\text{ref}} \equiv D_{\text{artery}} = 0.0033$ m and $\varrho_{\text{ref}} \equiv \varrho = 1050$ kg m $^{-3}$, the reference velocity is evaluated as $U_{\text{ref}} \equiv \bar{U}_{\text{inlet}} \cong 0.229$ m s $^{-1}$, whose value serves for the determination of parameter β . In all performed computations, we set $\beta = 2.5 \bar{U}_{\text{inlet}} \cong 0.573$ m s $^{-1}$, which approximately corresponds to $\beta = \max(\sqrt{v_1^2 + v_2^2 + v_3^2})$ in $\Omega \subset \mathbb{R}^3$. Our previous experiences with the application of the pseudo-compressibility method for the modelling of bypass hemodynamics confirm the suitability of such setting, which showed positive influence on the convergence history to the steady state solution.

In order to evaluate the shear-dependent viscosity $\eta(\dot{\gamma})$ in (8) for both non-Newtonian models, it is necessary to determine the scalar shear rate $\dot{\gamma}$ using the definition

$$\dot{\gamma} = 2 \sqrt{D_{\text{II}}} , \quad (9)$$

where D_{II} denotes the second invariant of rate of deformation tensor $\mathbf{D} = (\nabla \mathbf{v} + (\nabla \mathbf{v})^T) / 2$. The second invariant D_{II} is a scalar measure with suitable invariance properties with respect to the reference coordinate system and it can be expressed for the incompressible flow ($\text{tr} \mathbf{D} = 0$) as

$$D_{\text{II}} = \frac{1}{2} \text{tr} \mathbf{D}^2 = \frac{1}{2} d_{ij} d_{ij} , \quad (10)$$

where d_{ij} are the components of rate of deformation tensor \mathbf{D} given by

$$d_{ij} = \frac{1}{2} \left(\frac{\partial v_i}{\partial y_j} + \frac{\partial v_j}{\partial y_i} \right) , \quad i, j = 1, 2, 3 . \quad (11)$$

4. Numerical method

To solve the pseudo-transient system (5) of the incompressible NS equations, the cell-centred finite volume formulation of the central explicit fourth-stage Runge-Kutta (RK) time-stepping scheme defined on unstructured hexahedral computational grid, Fig. 1, is applied. In this numerical scheme, the pseudo-time has the role of iteration time with no physical significance. The applied computational grid consists of non-overlapping hexahedral finite volumes Ω_i with the boundary $\partial\Omega_i$, $i \in I$, where $I = \{1, 2, \dots, N\}$ is the index set. The finite volumes Ω_i cover the whole computational domain $\Omega \subset \mathbb{R}^3$, so that $\Omega = \bigcup_{i \in I} \Omega_i$. The boundary of hexahedral finite volume Ω_i is $\partial\Omega_i = \bigcup_{m=1}^6 \Gamma_{im}$, where Γ_{im} are the quadrilateral faces of Ω_i . According to this notation, the algorithm of the RK time-stepping scheme may be written as

$$\begin{aligned} \mathbf{w}_i^{(0)} &= \mathbf{w}_i^n , \\ \mathbf{w}_i^{(r)} &= \mathbf{w}_i^{(0)} - \alpha_r \Delta t \mathcal{R} \mathbf{w}_i^{(r-1)} + \mathcal{D} \mathbf{w}_i^{(0)} \quad \text{for } r = 1, 2, 3 , \\ \mathbf{w}_i^{(4)} &= \mathbf{w}_i^{(0)} - \frac{\Delta t}{6} \left(\mathcal{R} \mathbf{w}_i^{(0)} + 2 \mathcal{R} \mathbf{w}_i^{(1)} + 2 \mathcal{R} \mathbf{w}_i^{(2)} + \mathcal{R} \mathbf{w}_i^{(3)} \right) + \mathcal{D} \mathbf{w}_i^{(0)} , \\ \mathbf{w}_i^{n+1} &= \mathbf{w}_i^{(4)} , \end{aligned} \quad (12)$$

where $\alpha_1 = 0.5$, $\alpha_2 = 0.5$, $\alpha_3 = 1$, \mathbf{w}_i^n is the approximation of the vector \mathbf{w} over the finite volume Ω_i , $i \in I$ at the pseudo-time level n and \mathcal{D} is a dissipative operator. This scheme is

fourth-order accurate in time. The stationary residual $\mathcal{R} \mathbf{w}_i^{(r)}$ is defined as

$$\mathcal{R} \mathbf{w}_i^{(r)} = \frac{1}{|\Omega_i|} \left(\sum_{m=1}^6 \mathcal{F}_m^I(\mathbf{w}^{(r)}) \mathbf{S}_i^m - \sum_{m=1}^6 \mathcal{F}_m^V(\mathbf{w}^{(r)}) \mathbf{S}_i^m \right), \quad r = 0, 1, 2, 3,$$

where $|\Omega_i|$ denotes the volume of the hexahedral cell Ω_i and \mathbf{S}_i^m , $m = 1, \dots, 6$ are the outer vectors normal to the quadrilateral faces Γ_{im} of the finite volume Ω_i . The total inviscid numerical fluxes $\mathcal{F}_m^I = ((\mathbf{F}_1^I)_m, (\mathbf{F}_2^I)_m, (\mathbf{F}_3^I)_m)$ through the quadrilateral faces Γ_{im} , $m = 1, \dots, 6$ are evaluated at the cell faces as the average of the values from two neighbouring cells. For example, for the neighbouring cells Ω_i and Ω_j , which share a quadrilateral face Γ_{i1} (for $m = 1$) so that $\Gamma_{i1} = \partial\Omega_i \cap \partial\Omega_j$, the Cartesian component $(\mathbf{F}_1^I)_1$ of the total inviscid numerical flux \mathcal{F}_1^I through the quadrilateral face Γ_{i1} of the finite volume Ω_i may be written

$$\left(\mathbf{F}_1^I(\mathbf{w}^{(r)}) \right)_1 = \frac{1}{2} \left(\mathbf{F}_1^I(\mathbf{w}_i^{(r)}) + \mathbf{F}_1^I(\mathbf{w}_j^{(r)}) \right).$$

For the determination of the total viscous numerical fluxes $\mathcal{F}_m^V = ((\mathbf{F}_1^V)_m, (\mathbf{F}_2^V)_m, (\mathbf{F}_3^V)_m)$ through the quadrilateral faces Γ_{im} , $m = 1, \dots, 6$ the finite volume version of central differences is applied using dual cells in the form of octahedrons. For more details see e.g. [10].

In order to stabilize the numerical convergence process, an artificial viscosity term $\mathcal{D} \mathbf{w}$ has to be added to the numerical computation at each stage of the RK scheme. To save computational time, the artificial dissipation term is evaluated only once at the pseudo-time level n . With regard to the possibility that the added dissipation may negatively influence the shear-dependent viscosity of the fluid, the choice of a suitable artificial viscosity is crucial. In this study, we have chosen an artificial dissipation term

$$\mathcal{D} P = \frac{\varepsilon d^2}{\Delta t} \left(\frac{\partial^2 P}{\partial y_1^2} + \frac{\partial^2 P}{\partial y_2^2} + \frac{\partial^2 P}{\partial y_3^2} \right), \quad (13)$$

which is added to the continuity equation (to the first row of the system (5)). The artificial viscosity parameter $\varepsilon \in \mathbb{R}^+$ is a small constant (in our computations $\varepsilon \cong 10^{-8}$), d denotes the maximum body diagonal of the hexahedral finite volume Ω_i , $i \in I$ and Δt is the numerical integration time step. The second derivatives of P in (13) are computed using central differences of the second order accuracy.

5. Results

Regarding the objective of this study to investigate the blood's non-Newtonian behaviour in an occluded coronary 3D bypass model, Fig. 1, and to compare the obtained numerical results with the Newtonian flow, we prescribed the same steady boundary conditions for all three performed computations:

- **at the inlet** a fully developed velocity profile characterized by the inlet Reynolds number corresponding to the coronary artery ($Re_{\text{inlet}} = 230$)

$$v_1(r) = 2 \bar{U}_{\text{inlet}} \left[1 - \left(\frac{2r}{D_{\text{artery}}} \right)^2 \right], \quad \text{where } r = \sqrt{y_2^2 + y_3^2},$$

$$v_2 = 0 \text{ m s}^{-1},$$

$$v_3 = 0 \text{ m s}^{-1};$$

- **at the outlet** a constant pressure stated as the average arterial pressure ($p_2 = 12 \text{ kPa}$)
- **at the walls** the non-slip boundary condition.

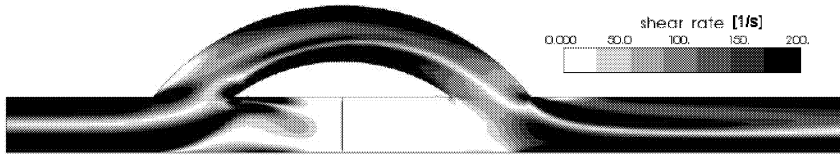


Fig.3: Distribution of shear rate $\dot{\gamma}$ at the longitudinal section through the occluded coronary 3D bypass model (Carreau-Yasuda model)

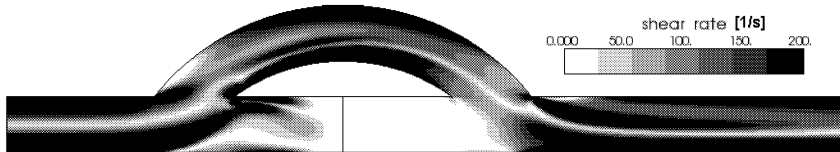


Fig.4: Distribution of shear rate $\dot{\gamma}$ at the longitudinal section through the occluded coronary 3D bypass model (Cross model)



Fig.5: Distribution of molecular viscosity $\eta(\dot{\gamma})^{(1)}$ at the longitudinal section through the occluded coronary 3D bypass model (Carreau-Yasuda model)



Fig.6: Distribution of molecular viscosity $\eta(\dot{\gamma})^{(2)}$ at the longitudinal section through the occluded coronary 3D bypass model (Cross model)

According to the definitions of the Carreau-Yasuda model (1) and the Cross model (2), the evaluation of the molecular viscosity is dependent on the determination of shear rate inside the considered bypass model with occluded native artery. For a better understanding, the resulting distributions of shear rate $\dot{\gamma}$ at the longitudinal section of the 3D bypass model in the case of the Carreau-Yasuda model and of the Cross model are shown in Fig. 3 and Fig. 4, respectively. According to our expectations, it is visible that the low values of shear rate are localized mainly around the occlusion, where the fluid is mostly motionless, and inside the main stream. The value range in both figures had to be lowered due to extremely high values of shear rate (around $3 \times 10^3 \text{ s}^{-1}$) in the regions of both proximal and distal anastomoses. On the one hand very high values of shear rate and on the other hand values almost equal to zero are the main reason for the unsuitability of the standard power-law model in our case. The standard power-law model is known to have problems with high gradients and infinite viscosity predictions. Therefore, the selection of the Carreau-Yasuda

model and the Cross model, which both have lower and upper viscosity limits, seems like the optimal solution regarding the non-Newtonian blood flow through our considered coronary bypass model.

Considering the reached value range of shear rate $\dot{\gamma}$, which is mostly restricted to values around 150 s^{-1} for both non-Newtonian flows, see Fig. 3 and Fig. 4, the computed distribution of the molecular viscosities for the Carreau-Yasuda model, Fig. 5, and for the Cross model, Fig. 6, do not differ very much from each other inside the occluded coronary bypass model. In reference to the graph in Fig. 2, where the dependence of molecular viscosity on shear rate is shown, it is apparent that by high values of shear rate the viscosity of both non-Newtonian models is very similar and almost equal to the viscosity of the Newtonian fluid. The fact is also supported by the resulting flow fields of both the Carreau-Yasuda model and the Cross model in comparison with the Newtonian flow as is visible in Tab. 1. In the table, the velocity isolines are shown at several selected cross-sections for all three considered cases. For the position of the selected cross-sections along the occluded coronary bypass model, see Fig. 7. Another possibility to compare the results is in the form of velocity profiles, which are shown in Fig. 8 for the Newtonian fluid and in Fig. 9 and Fig. 10 for the non-Newtonian fluids. Once again the differences between the Newtonian and non-Newtonian flows are rather insignificant.

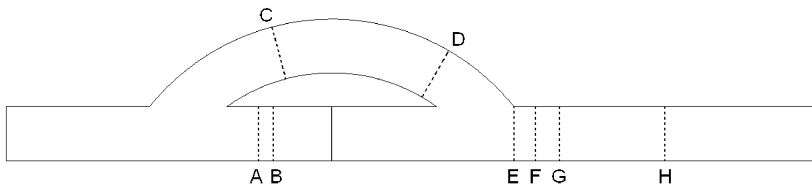


Fig. 7: Positions of selected cross-sections along the occluded 3D bypass model

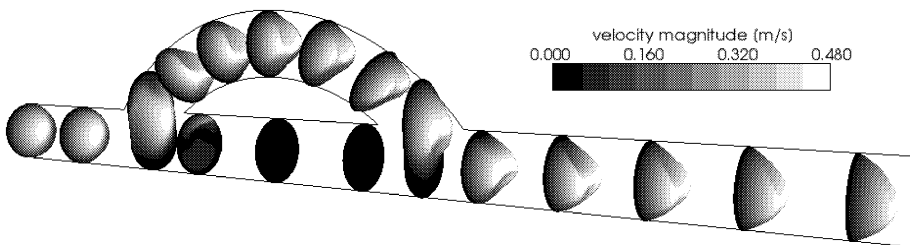


Fig. 8: Velocity profiles at several cross-sections in the occluded coronary bypass for the Newtonian flow

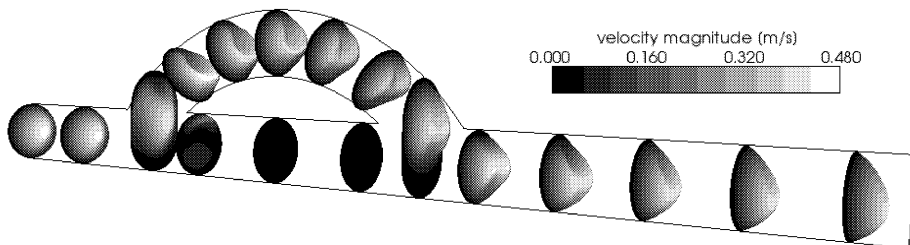


Fig. 9: Velocity profiles at several cross-sections in the occluded coronary bypass for the non-Newtonian flow (Carreau-Yasuda model)

cross-section	non-Newtonian fluid (Carreau-Yasuda model)	Newtonian fluid	non-Newtonian fluid (Cross model)
A			
B			
C			
D			
E			
F			
G			
H			

Tab.1: Velocity isolines at selected cross-sections marked in Fig.7

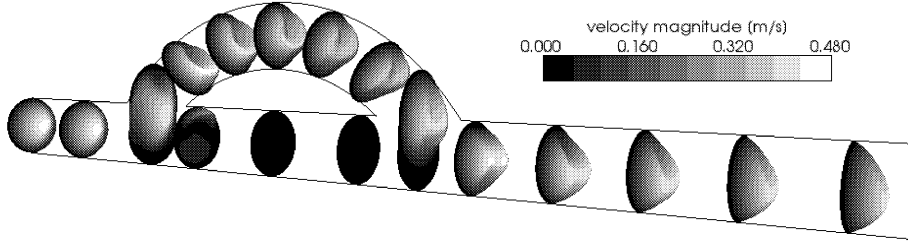


Fig.10: Velocity profiles at several cross-sections in the occluded coronary bypass for the non-Newtonian flow (Cross model)

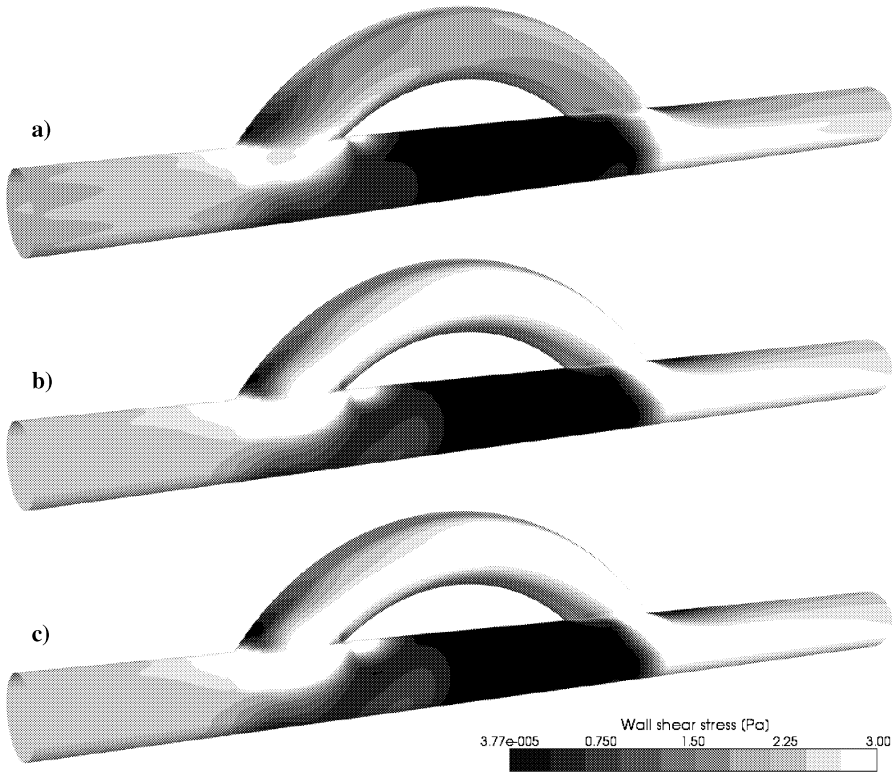


Fig.11: Wall shear stress τ_W – a) Newtonian flow, b) non-Newtonian flow (Carreau-Yasuda model), c) non-Newtonian flow (Cross model)

Even though the obtained flow fields from both non-Newtonian models seem relatively similar with the case of Newtonian flow, the values of shear stress at the model walls demonstrate a significant increase at the proximal and distal anastomoses and inside the bypass graft for both generalized Newtonian models compared to the Newtonian flow, Fig. 11.

6. Conclusions

In order to investigate the blood's non-Newtonian behaviour in an idealized occluded coronary 3D bypass model, several numerical computations were performed with the application of two well-known macroscopic non-Newtonian models (the Carreau-Yasuda model and the Cross model). In our case, the use of the standard power-law model was avoided

due to extremely high and low values of shear rate, which for the power-law model may lead to problems with high gradients and infinite viscosity predictions at both anastomoses and around the occlusion. Compared to other studies, which also dealt with the non-Newtonian bypass hemodynamics, a complete bypass model was considered applying average physiological parameters connected with coronary arteries.

The obtained numerical results showed small differences in the velocity distribution by comparing the non-Newtonian flows with the Newtonian one. The in sense of human biomechanics high Reynolds number for the blood flow through a coronary artery ($Re_{\text{inlet}} = 230$), is probably the main reason for relatively high shear rates leading to small viscosity increase in the entire bypass model and therefore, to small changes in the resulting flow field. On the other hand, the distribution of wall shear stress for the case of considered non-Newtonian flows demonstrated significant dissimilarities at the graft walls and at both anastomoses in comparison with the Newtonian flow. Considering the undeniable importance of wall shear stress as one of the main hemodynamical factors by the analysis of bypass hemodynamics in connection with the late graft failure, the obtained values indicate a significant role of blood's non-Newtonian behaviour even in medium-sized arteries such as the coronary artery.

Acknowledgement

This investigation was supported by the research project MSM 4977751303 of the Ministry of Education, Youth and Sports of the Czech Republic.

References

- [1] Bertolotti C., Deplano V.: Three-dimensional numerical simulations of flow through a stenosed coronary bypass, *J. Biomech.* 33(8): 1011–1022, 2000
- [2] Chen J., Lu X.-Y., Wang W.: Non-Newtonian effects of blood flow on hemodynamics in distal vascular graft anastomoses, *J. Biomech.* 39(11): 1983–1995, 2006
- [3] Chorin A.J.: A numerical method for solving incompressible viscous flow problems, *J. Comput. Physics* 2: 12–26, 1967
- [4] Gray J.D., Owen I., Escudier M.P.: Dynamic scaling of unsteady shear-thinning non-Newtonian fluid flows in a large-scale model of a distal anastomosis, *Exp. Fluids* 43: 535–546, 2007
- [5] Henry F.S., Küpper C., Lewington N.P.: Simulation of flow through a Miller cuff bypass graft, *Comput. Methods Biomech. Biomed. Eng.* 5(3): 207–217, 2002
- [6] Janela J., Saqueira A.: High accuracy semi-analytical solutions for generalized Newtonian flows, In: *Proceedings of the conference Topical problems of fluid mechanics*, Prague, 2007
- [7] Lee D., Su J.M., Liang H.Y.: A numerical simulation of steady flow fields in a bypass tube, *J. Biomech.* 34(11): 1407–1416, 2001
- [8] Leuprecht A., Perktold K.: Computer simulation of non-Newtonian effects of blood flow in large arteries, *Comput. Methods Biomech. Biomed. Eng.* 4(2): 149–163, 2000
- [9] Leuprecht A., Perktold K., Prosi M., Berk T., Trubel W., Schima H.: Numerical study of hemodynamics and wall mechanics in distal end-to-side anastomoses of bypass grafts, *J. Biomech.* 35(2): 225–236, 2002
- [10] Vimmr J., Jonášová A.: Analysis of blood flow through a three-dimensional bypass model, *J. Appl. Comput. Mech.* 1(2): 693–702, 2007

Received in editor's office: March 28, 2008

Approved for publishing: May 15, 2008